

^{12}C properties with evolved chiral three-nucleon interactions

P. Maris,^{1,*} J.P. Vary,^{1,†} A. Calci,^{2,‡} J. Langhammer,^{2,§} S. Binder,^{2,¶} and R. Roth^{2,**}

¹*Department of Physics and Astronomy, Iowa State University, Ames, IA 50011, USA*

²*Institut für Kernphysik, Technische Universität Darmstadt, 64289 Darmstadt, Germany*

(Dated: May 10, 2014)

We investigate selected static and transition properties of ^{12}C using *ab initio* No-Core Shell Model (NCSM) methods with chiral two- and three-nucleon interactions. We adopt the Similarity Renormalization Group (SRG) to assist convergence including up to three-nucleon (3N) contributions. We examine the dependences of the ^{12}C observables on the SRG evolution scale and on the model-space parameters. We obtain nearly converged low-lying excitation spectra. We compare results of the full NCSM with the Importance Truncated NCSM in large model spaces for benchmarking purposes. We highlight the effects of the chiral 3N interaction on several spectroscopic observables. The agreement of some observables with experiment is improved significantly by the inclusion of 3N interactions, e.g., the B(M1) from the first $J^\pi T = 1^+1$ state to the ground state. However, in some cases the agreement deteriorates, e.g., for the excitation energy of the first 1^+0 state, leaving room for improved next-generation chiral Hamiltonians.

PACS numbers: 21.30.-x, 05.10.Cc, 13.75.Cs

I. INTRODUCTION

No-Core Configuration Interaction methods have advanced rapidly in recent years to make it feasible to accurately solve fundamental problems in nuclear structure and reaction physics (e.g., see Refs. [1–11]). At the same time, significant theoretical advances regarding the underlying Hamiltonians, constructed within chiral effective field theory (EFT), provide a foundation for nuclear many-body calculations rooted in QCD [12, 13]. In order to improve the convergence behavior of the many-body calculations we employ a consistent unitary transformation of the chiral Hamiltonians. Here we use the Similarity Renormalization Group (SRG) [14–18] approach that provides a straightforward and flexible framework for consistently evolving (softening) the Hamiltonian and other operators, including three-nucleon interactions [8, 19–21].

The goal of this paper is twofold. First, we aim to provide results for ^{12}C spectra and other observables using realistic chiral nucleon-nucleon (NN) plus three-nucleon (3N) interactions with uncertainty estimates where feasible. Second, we provide benchmark comparisons between the full No-Core Shell Model (NCSM) [1–3] and the Importance Truncated No-Core Shell Model (IT-NCSM) [7–9, 21].

Previous investigations of ^{12}C with chiral NN+3N interactions, softened with the SRG approach, have mainly focused on the ground-state energy [8, 20] and its convergence properties. One of the directions in which the

present work extends these earlier efforts is by investigating a wider set of observables including selected electromagnetic transitions and the lowest-lying negative parity states. Our initial results for the 2^+ and 4^+ rotational excited states were presented in Ref. [22].

We limit our investigations to a single form of the chiral NN+3N interaction. We use the chiral NN interaction at N^3LO with 500 MeV/c cutoff from Ref. [23] together with the 3N potential at N^2LO [24] in the local form of Ref. [25] with 500 MeV/c cutoff and low-energy constants determined entirely in the three-nucleon sector [26]. This is also the Hamiltonian used in Refs. [8, 19–21, 27]. We evolve this Hamiltonian using the free-space SRG to three representative flow parameters or momentum scales to examine the scale-dependence of our results. As in the earlier applications, we retain the induced many-body interaction through the three-nucleon level and neglect induced four- and multi-nucleon interactions.

In Section II, we briefly review the formalism and summarize related results from previous work. The results for selected ^{12}C observables are presented in Section III. Section IV presents benchmarks of the IT-NCSM and NCSM. Finally, Section V summarizes our conclusions and provides perspectives on future efforts.

II. THEORETICAL BACKGROUND

A. NCSM and IT-NCSM

We employ two related *ab initio* methods to solve for the properties of ^{12}C . In the first approach, the NCSM, we follow Refs. [1–3] where, for a chosen NN and 3N interaction (either without or with SRG evolution) we diagonalize the resulting many-body Hamiltonian in a sequence of truncated harmonic-oscillator (HO) basis spaces. The basis spaces are characterized by two parameters: N_{max} specifies the maximum number of total

* pmaris@iastate.edu

† jvary@iastate.edu

‡ angelo.calci@physik.tu-darmstadt.de

§ joachim.langhammer@physik.tu-darmstadt.de

¶ sven.binder@physik.tu-darmstadt.de

** robert.roth@physik.tu-darmstadt.de

HO quanta beyond the HO Slater determinant with all nucleons occupying their lowest-allowed orbitals and $\hbar\Omega$ specifies the HO energy. The goal is to achieve convergence as indicated by independence of these two basis parameters, either directly or by extrapolation [4].

In the second approach, the IT-NCSM, we follow Refs. [7–9, 21] where subspaces of the N_{\max} -truncated spaces are dynamically selected according to a measure derived from perturbation theory. The IT-NCSM uses this derived importance measure κ_ν for the individual many-body basis states and retains only states with $|\kappa_\nu|$ above a threshold κ_{\min} in the model space. Through a variation of this threshold and an *a posteriori* extrapolation $\kappa_{\min} \rightarrow 0$ the contribution of discarded states is recovered. We use the sequential update scheme discussed in Refs. [7, 21], which connects to the full NCSM model space and, thus, to the exact NCSM results in the limit of vanishing threshold. In the following we report threshold-extrapolated results of the IT-NCSM at each N_{\max} including an estimate for the extrapolation uncertainties. In addition, we compare the IT-NCSM results with the NCSM results in model spaces where we evaluate results from both approaches.

B. Chiral NN+3N Interactions

Chiral EFT has developed into a standard approach for the construction of NN and 3N interactions with low-energy constants (LECs) fitted to NN and 3N data. As mentioned above, we adopt the chiral EFT potential at N³LO with 500 MeV/c cutoff from Ref. [23] together with an 3N potential at N²LO [24] in the local form of Ref. [25] as this Hamiltonian was adopted for a range of *ab initio* calculations of light and medium-mass nuclei and, in particular, was used in previous works for ¹²C. For the LECs introduced by the 3N interaction at N²LO, we adopt the values fitted to the $A = 3$ binding energies and tritium half-life [28]. That is, we adopt $c_D = -0.2$ and $c_E = -0.205$ for a cutoff of 500 MeV/c.

The first paper to report results for ¹²C with chiral NN+3N interactions (with a different choice for c_D and c_E) is Ref. [29]. That work employed the NCSM with the Okubo-Lee-Suzuki (OLS) transformation method [30, 31] to improve convergence and presented natural parity results up through $N_{\max} = 6$ basis spaces. We considerably extend this span of basis spaces with the present work and include the lowest unnatural parity states. Moreover, we use the SRG evolution to soften the interaction instead of the OLS transformation. The SRG-evolved chiral NN+3N Hamiltonian adopted here was first applied in IT-NCSM calculations for the ground-state and excitation spectra of ¹²C in Ref. [8].

C. SRG Evolution

In the SRG framework the unitary transformation of an operator, e.g. the Hamiltonian, is formulated in terms of a flow equation

$$\frac{d}{d\alpha} H_\alpha = [\eta_\alpha, H_\alpha] \quad (1)$$

with a continuous flow parameter α . The initial condition for the solution of this flow equation is given by the 'bare' chiral Hamiltonian. The physics of the SRG evolution is governed by the anti-hermitian generator η_α . A specific form widely used in nuclear physics [17, 32] is given by

$$\eta_\alpha = m_N^2 [T_{\text{int}}, H_\alpha] \quad (2)$$

where m_N is the nucleon mass and T_{int} is the intrinsic kinetic-energy operator. This generator drives the Hamiltonian towards a diagonal form in a basis of eigenstates of the intrinsic kinetic energy, i.e., towards a diagonal in momentum space.

Along with the reduction in the coupling of low-momentum and high-momentum components by the Hamiltonian, the SRG induces many-body operators beyond the particle rank of the initial Hamiltonian. In principle, all the induced terms up to the A-body level are to be retained in order that the transformation remains unitary and the spectrum of the Hamiltonian in an exact A-body calculation is independent of the flow parameter. In practice we have to truncate the evolution at a low particle rank (typically, two or three nucleons), which violates formal unitarity. In this situation we can use the flow parameter as a diagnostic tool to quantify the contribution of omitted many-body terms [8, 21].

Throughout this work, we employ the SRG evolution at the three-nucleon level and neglect four- and multi-nucleon induced interactions. For the application in the NCSM it is convenient to solve the flow equation for the three-body system using a HO Jacobi-coordinate basis [21, 33]. The intermediate sums in the three-body Jacobi basis are truncated at $N_{\max} = 40$ for channels with $J \leq 5/2$ and ramp down linearly to $N_{\max} = 24$ for $J \geq 13/2$. Based on this and the corresponding solution of the flow equation in two-body space (using either a partial-wave momentum- or harmonic-oscillator representation) we extract the irreducible two- and three-body terms of the Hamiltonian for the use in A-body calculations. A detailed discussion of the SRG evolution in the 3N sector with benchmarks of the truncations involved can be found in Ref. [21].

D. Computational Aspects of the Many-Body Calculations

In our many-body calculations, the size of the largest feasible model space is constrained by the total number of three-body matrix elements required as well as by

the number of many-body matrix elements that are computed and stored for the iterative Lanczos diagonalization procedure. Through a JT -coupled scheme and an efficient on-the-fly decoupling during the calculation of the many-body Hamiltonian matrix [8, 21, 34, 35], the limit arising from the handling of $3N$ matrix-elements has been pushed to significantly larger many-body model spaces. At present, for mid p-shell nuclei the number of non-zero many-body matrix elements defines the maximum N_{\max} that can be reached in NCSM calculations.

For the full NCSM calculations we employ the MFDn code [36–38] that is highly optimized for parallel computing. The calculations were performed on the Cray XE6 Hopper at NERSC, using up to about 100 TB of memory across 76,320 cores; and on the Cray XK6 Jaguar at ORNL, using 180 TB of memory across 112,224 cores, taking about 40 minutes per $\hbar\Omega$ -value at $N_{\max} = 8$ for 8 converged eigenvalues. MFDn has been demonstrated to scale well on these platforms for these types of runs; scaling runs have been performed up to 261,120 cores on the Cray XK6 Jaguar [39].

The IT-NCSM calculations are performed with a dedicated code [7, 21] that has been developed to accommodate the specific demands of an importance-truncated calculation in a framework optimized for parallel performance. Due to the reduction of the model-space dimension resulting from the importance truncation, typically by two orders of magnitude, the many-body Hamiltonian matrix is significantly smaller and the memory needs are drastically reduced. An IT-NCSM run targeting 8 positive-parity states of ^{12}C in an $N_{\max} = 8$ space for $\alpha = 0.0625 \text{ fm}^4$ and $\hbar\Omega = 20 \text{ MeV}$ takes about 10 hours wall time on 160 nodes on the Cray XE6 Hopper at NERSC and needs a total of 2.5 TB of memory for storing the many-body Hamiltonian matrix in the largest importance-truncated space. This run includes the construction of the importance-truncated space, the computation of the many-body Hamiltonian matrix, and the separate solution of the eigenvalue problems for 15 different values of the importance threshold κ_{\min} . Further details on the set-up of the IT-NCSM calculations are discussed in Sec. IV.

III. RESULTS

A. Excitation Spectra of ^{12}C

We first investigate the dependence of the excitation spectra of ^{12}C on the SRG flow parameter. Starting from the initial chiral NN+3N interaction, we evolve the Hamiltonian up to a specific flow-parameter α , consistently including two- and three-body terms, but neglecting SRG-induced four- and multi-nucleon interactions. Note that even in cases, where we omit the initial chiral 3N interaction for comparison purposes, we always include the SRG-induced 3N terms in our calculations, leading to the so-called NN+3N-induced Hamiltonian.

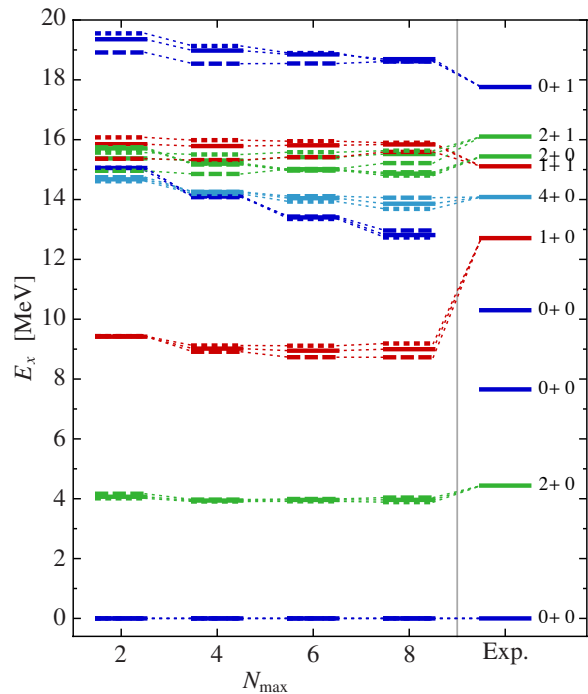


FIG. 1. (color online) Excitation spectra of ^{12}C with the chiral NN+3N interactions for three different SRG evolution scales as a function of N_{\max} at $\hbar\Omega = 20 \text{ MeV}$ compared with experiment. The solid line for each calculated level represents results with $\alpha = 0.0625 \text{ fm}^4$. The long dashed line represents NCSM results with $\alpha = 0.08 \text{ fm}^4$ and the short dashed line represents NCSM results with $\alpha = 0.04 \text{ fm}^4$.

Figure 1 shows the behavior of the excitation energies obtained in the full NCSM with increasing N_{\max} for three values of the SRG flow parameter $\alpha = (0.04, 0.0625, 0.08) \text{ fm}^4$, corresponding to momentum scales $\lambda_{\text{SRG}} = \alpha^{-1/4} = (2.24, 2.0, 1.88) \text{ fm}^{-1}$. The spread of converged results with the SRG flow parameter will provide an indication of the relevance of the neglected SRG-induced four- and multi-nucleon interactions. The absolute ground-state energy starts to show a non-negligible flow-parameter dependence for ^{12}C as discussed in detail in Refs. [8, 21]. The excitation energies at fixed $\hbar\Omega$ are rather insensitive to the choice of the flow parameter. The ground-state and excitation energies, as well as additional observables, are provided in Table I.

In Fig. 2 we display the excitation spectra of ^{12}C at two values of $\hbar\Omega$ as a function of N_{\max} . The spread of the results with $\hbar\Omega$ indicates the lack of convergence with respect to increasing N_{\max} . However, the movement of the excitation energies with increasing N_{\max} is consistent with eventual convergence.

From Figs. 1 and 2 one sees that the convergence patterns are well-enough established to conclude that the $J^\pi T = 2^+0$ and 4^+0 rotational states are reasonably well reproduced [22]. This is not so surprising in light of recent successful *ab initio* descriptions of collective motion in light nuclei [32, 40, 41]. However, the 1^+0 is at least

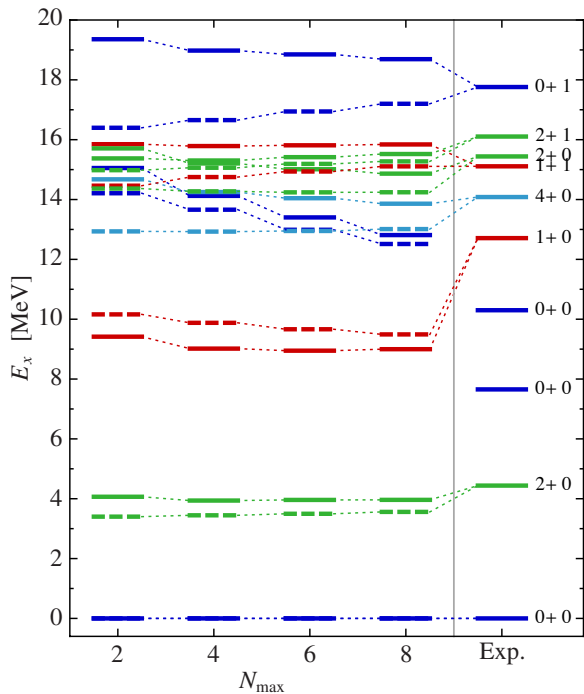


FIG. 2. (color online) Excitation spectra of ^{12}C with the chiral NN+3N interactions, for two different $\hbar\Omega$ values, as a function of N_{max} at $\alpha = 0.0625 \text{ fm}^4$ compared with experiment. The solid line for each calculated state represents results with $\hbar\Omega = 20 \text{ MeV}$. The long dashed line represents results with $\hbar\Omega = 16 \text{ MeV}$.

3 MeV too low as seen in previous ^{12}C works using the NCSM with chiral NN+3N interactions [8, 29]. In addition, we re-confirm the issue that our basis spaces are insufficient to reproduce the first excited 0^+0 state, the Hoyle state [42, 43]. Whether the third excited state at $N_{\text{max}} = 8$, our first excited 0^+0 state, continues its downward trend towards the Hoyle state at higher N_{max} values remains a challenge for the future.

We note that recent lattice simulations with chiral EFT interactions through N^2LO observe the Hoyle state at approximately the correct excitation energy [44, 45]. It will be interesting to see if the lattice simulated Hoyle state remains in good agreement with experiment at chiral N^3LO and with a range of lattice spacings. In addition, it will be interesting to see where the other low-lying states appear in comparison with experiment.

In order to examine the role of the 3N interaction, we compare in Fig. 3 the ^{12}C spectra at SRG evolution scale $\alpha = 0.0625 \text{ fm}^4$ and $\hbar\Omega = 20 \text{ MeV}$ obtained without and with initial chiral 3N interactions. In both cases the SRG evolution is performed up to the three-body level: without the initial 3N interaction this leads to the NN+3N-induced Hamiltonian while with the initial 3N we obtain the NN+3N-full Hamiltonian as used above. We observe that the impact of the initial chiral 3N interaction is very different for the various excited states. Whereas the excitation energies of most states are shifted

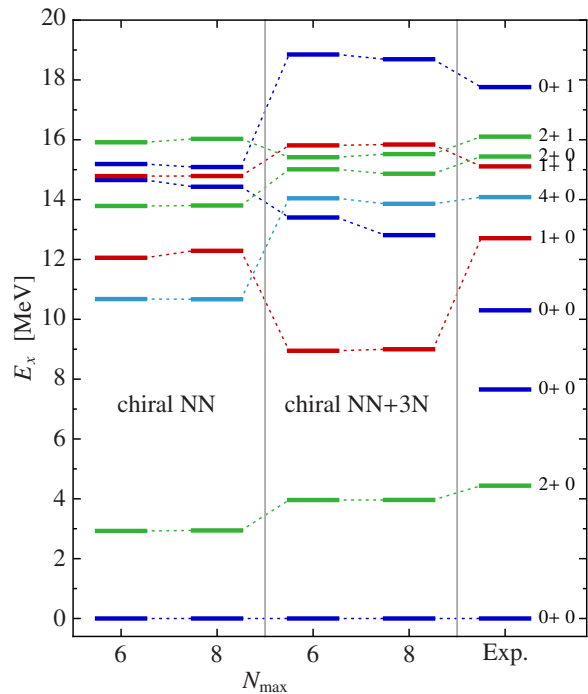


FIG. 3. (color online) Excitation spectra of ^{12}C without and with initial chiral 3N interaction for two different N_{max} values, compared with experiment. These NCSM results are calculated at $\hbar\Omega = 20 \text{ MeV}$ for flow-parameter $\alpha = 0.0625 \text{ fm}^4$.

by about 1 MeV, some states exhibit a much stronger sensitivity to the initial 3N interaction. Among the latter are the first 1^+0 and the first 0^+1 states. The excitation energy of the first 1^+0 is reduced by more than 3 MeV by the 3N interaction and the excitation energy of the first 0^+1 state is increased by more than 3 MeV. These large shifts indicate that these states are strong candidates for sensitive probes of chiral 3N interactions, particularly for the next-generation consistent chiral NN+3N Hamiltonians at N^3LO [46]. Note, however, that these excitation energies are not yet converged as seen in the N_{max} and $\hbar\Omega$ -dependence of Fig. 2.

Another noteworthy effect of including the full 3N interaction seen in Fig. 3 is to increase the excitation energies of the lowest rotational excitations, the 2^+0 and 4^+0 , by about 30%. This increase may be understood as a similar decrease in the moment of inertia brought about by the increase in binding energy. Indeed, the ground state rms radius and quadrupole moments are decreased by the inclusion of the full 3N interaction as discussed below.

We note that the results at $N_{\text{max}} = 6$ are similar, both in the locations of excited states and in the changes with the inclusion of the chiral 3N interaction, with the previous $N_{\text{max}} = 6$ results of Ref. [29]. This similarity is remarkable considering the different $\hbar\Omega$ values and the different renormalization schemes—Ref. [29] used $\hbar\Omega = 15 \text{ MeV}$ and the OLS transformation.

B. Survey of Observables

In addition to the spectra shown in the figures above, we present in Table I the ground-state energy, selected excitation energies and a survey of electromagnetic observables in ^{12}C for one choice of SRG flow-parameter, $\alpha = 0.0625 \text{ fm}^4$, and one choice of HO basis frequency, $\hbar\Omega = 20 \text{ MeV}$. While many cases were generated to perform our systematic survey and prepare the figures, we have chosen this one representative case, with a moderate value of the SRG evolution scale, to present in more detail. We tabulate these results in order to stimulate detailed comparisons with other methods and other Hamiltonians. In addition, we specify the IT-NCSM results for the benchmark comparison discussed in detail in the Sec. IV.

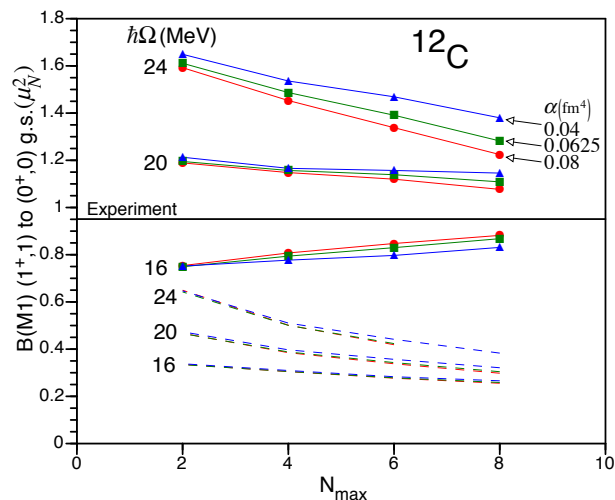


FIG. 4. (color online) Reduced magnetic dipole transition matrix element from the 1^+1 to the ground state of ^{12}C (in units of μ_N^2) as a function of N_{max} at three different SRG evolution scales and three different HO basis frequencies. The solid and dashed lines present the results obtained with and without the initial chiral 3N interaction, respectively.

In order to more completely understand the basis space ($N_{\text{max}}, \hbar\Omega$) dependence as well as the flow-parameter dependence of two selected electromagnetic observables, we present these results as a function of N_{max} in Figs. 4 and 5.

The example of the B(M1) from the 1^+1 to the ground state has previously been identified as receiving about a factor of three enhancement when 3N interactions are included [50]. This earlier work used the Tucson-Melbourne TM'(99) interaction [51] in NCSM calculations up through $N_{\text{max}} = 6$ to establish this enhancement. This enhancement has been confirmed with chiral NN+3N interactions in NCSM calculations also through $N_{\text{max}} = 6$ using the OLS renormalization approach [29]. In Fig. 4 we reconfirm this result with chiral NN+3N interactions up through $N_{\text{max}} = 8$ and show the sensi-

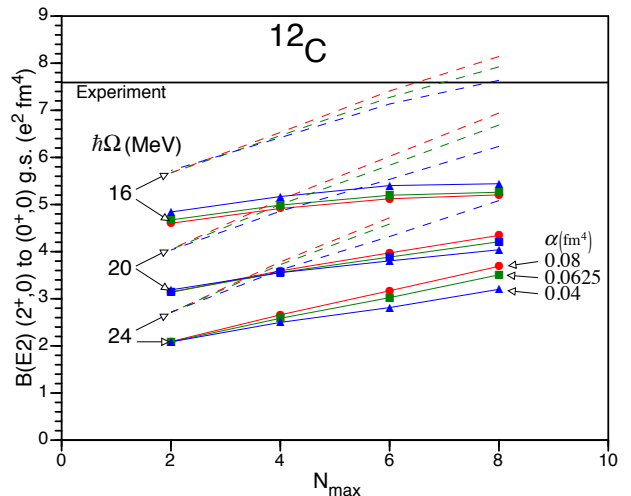


FIG. 5. (color online) Reduced electric quadrupole transition matrix element from the 2^+0 to the ground state of ^{12}C (in units of $e^2 \text{ fm}^4$) as a function of N_{max} at three different SRG evolution scales and three different HO basis frequencies. The solid and dashed lines present the results obtained with and without the initial chiral 3N interaction, respectively.

tivity to the SRG flow-parameter and to the basis-space parameters ($N_{\text{max}}, \hbar\Omega$). Clearly, these dependences are weak enough that the general conclusion remains—this B(M1) is strongly enhanced by 3N interactions and the amount of enhancement is roughly independent of the adopted Hamiltonian.

Contrasting the favorable convergence picture for the B(M1), other observables that are sensitive to the extent of the wavefunction, such as rms radii, quadrupole moments and B(E2)'s, are not well converged (see Table I). Of course, the radial extent is sensitive to the binding energy relative to the first threshold which is the 3α threshold at about 7 MeV experimentally. This allows an intuitive interpretation of our results for the B(E2) from the lowest 2^+0 to the ground state, see Fig. 5. One of the effects of the inclusion of the chiral 3N interaction is that the 3α threshold is pushed to higher excitation energies. Without the chiral 3N interaction, both, ^4He and ^{12}C are underbound and we find the 3α threshold at too low excitation energies. The inclusion of the 3N interaction increases the binding energy of ^4He and of ^{12}C such that the 3α threshold is pushed to higher excitation energies. Not surprisingly, the changes in the B(E2)s are well correlated with the changes in the binding and threshold energies. Also, the changes in the B(E2)s are well correlated with the changes in the ground state rms radius and the quadrupole moment of the first 2^+0 .

One has to keep in mind, however, that two components are still missing in the present, state-of-the-art calculations of electromagnetic observables: First, we should transform the electromagnetic operators consistently with the Hamiltonian in the SRG evolution. How-

N_{\max}	chiral NN			chiral NN+3N			Experiment
	(4,5)	(6,7)	(8,9)	(4,5)	(6,7)	(8,9)	
$E(0_1^+0)$ [MeV]	-68.123	-73.483	-76.617	-85.756	-92.182	-95.761	-92.161
	-68.123	-73.544(40)	-76.238(90)	-85.756	-92.229(16)	-95.662(45)	
$r_p(0_1^+0)$ [fm]	2.217	2.263	2.305	2.120	2.136	2.149	2.35(2)
	2.217	2.264(1)	2.284(10)	2.120	2.136(1)	2.140(9)	
$Q(2_1^+0)$ [e fm ²]	4.735	5.107	5.451	3.936	4.136	4.321	6(3)
	4.735	5.129(30)	5.191(200)	3.936	4.155(27)	4.232(160)	
$E_x(2_1^+0)$ [MeV]	2.918	2.926	2.943	3.939	3.960	3.962	4.439
	2.918	2.921(6)	2.881(12)	3.939	3.962(4)	3.980(19)	
$E_x(0_2^+0)$ [MeV]	15.008	14.655	14.430	14.122	13.402	12.812	7.654
	15.008	14.667(15)	14.436(26)	14.121	13.426(16)	13.066(38)	
$E_x(1_1^+0)$ [MeV]	11.886	12.056	12.288	9.017	8.948	8.998	12.710
	11.886	12.050(13)	12.116(23)	9.018	8.951(9)	8.891(20)	
$E_x(4_1^+0)$ [MeV]	10.704	10.676	10.670	14.250	14.044	13.860	14.083
	10.704	10.682(7)	10.703(10)	14.250	14.052(8)	14.015(33)	
$E_x(1_1^+1)$ [MeV]	14.819	14.786	14.788	15.787	15.812	15.841	15.110
	14.819	14.774(15)	14.712(32)	15.787	15.820(8)	15.833(23)	
$E_x(2_2^+0)$ [MeV]	13.834	13.787	13.803	15.206	15.012	14.865	(15.44)
	13.834	13.784(9)	13.719(10)	15.206	15.017(4)	14.950(29)	
$E_x(2_1^+1)$ [MeV]	15.781	15.916	16.030	15.304	15.416	15.521	16.106
	—	—	—	15.305	15.419(9)	15.430(40)	
$E_x(0_1^+1)$ [MeV]	15.359	15.189	15.088	18.978	18.850	18.691	17.760
	15.359	15.182(9)	15.020(40)	—	—	—	
$E(3_1^-0)$ [MeV]	-55.010	-61.249	—	-70.460	-77.336	—	-82.520
	-55.010	-61.182(150)	-62.883(400)	-70.460	-77.464(120)	-79.961(400)	
$E_x(3_1^-0)$ [MeV]	13.113	12.234	—	15.296	14.846	—	9.641
	13.113	12.362(170)	13.355(450)	15.297	14.765(150)	15.701(450)	
$E_x(1_1^-0)$ [MeV]	16.079	15.079	—	17.703	17.089	—	10.844
	16.079	15.217(170)	15.937(450)	17.703	16.999(150)	17.688(450)	
$E_x(2_1^-0)$ [MeV]	17.081	16.182	—	17.937	17.429	—	11.828
	17.080	16.304(170)	17.059(450)	17.937	17.305(150)	17.905(450)	
$E_x(4_1^-0)$ [MeV]	16.944	16.122	—	19.030	18.579	—	(13.352)
	16.943	16.282(170)	17.348(450)	19.030	18.508(150)	19.482(450)	
B(E2;2 ₁ ⁺ 0 → 0 ₁ ⁺ 0) [e^2 fm ⁴]	5.001	5.834	6.689	3.558	3.885	4.210	7.59(42)
	5.001	5.844(18)	6.504(90)	3.558	3.894(8)	4.080(75)	
B(M1;1 ₁ ⁺ 0 → 0 ₁ ⁺ 0) [μ_N^2]	0.0032	0.0030	0.0030	0.0080	0.0079	0.0078	0.0145(21)
	0.0032	0.0030(1)	0.0032(2)	0.0079	0.0078(1)	0.0082(3)	
B(M1;1 ₁ ⁺ 1 → 0 ₁ ⁺ 0) [μ_N^2]	0.388	0.343	0.304	1.157	1.139	1.109	0.951(20)
	0.388	0.343(1)	0.329(6)	1.157	1.135(5)	1.143(36)	
B(E2;2 ₁ ⁺ 1 → 0 ₁ ⁺ 0) [e^2 fm ⁴]	0.308	0.293	0.241	0.437	0.442	0.436	0.65(13)
	—	—	—	0.437	0.440(7)	0.444(18)	

TABLE I. Calculated and experimental total energies E , excitation energies E_x , point-proton rms radii r_p , quadrupole moments Q , as well as E2 transitions B(E2), and M1 transitions B(M1) of ¹²C. The first 3 columns correspond to results for the initial chiral NN interaction (still including SRG-induced 3N-terms) while the next 3 columns correspond to chiral NN+3N interaction using an SRG evolution scale $\alpha = 0.0625$ fm⁴ ($\lambda_{\text{SRG}} = 2.0$ fm⁻¹) and $\hbar\Omega = 20$ MeV. Columns of theoretical results are labelled by pairs of natural and unnatural parity basis spaces characterized by their N_{\max} values. The first row of each observable is obtained with the NCSM while the second row is obtained from the IT-NCSM. The uncertainty extracted from the threshold extrapolation of the IT-NCSM results as discussed in the text are quoted in parenthesis; for $N_{\max} = (4, 5)$ the full space was used. The experimental values are taken from Ref. [47–49].

ever, so far we only employ the bare operators. Second, we should include the two-body currents derived in chiral EFT. However, so far we only employ the one-body part. These two corrections are not likely to affect the qualitative discussion present here, but they will play a role in future precision calculations of electromagnetic observables.

C. Negative Parity States

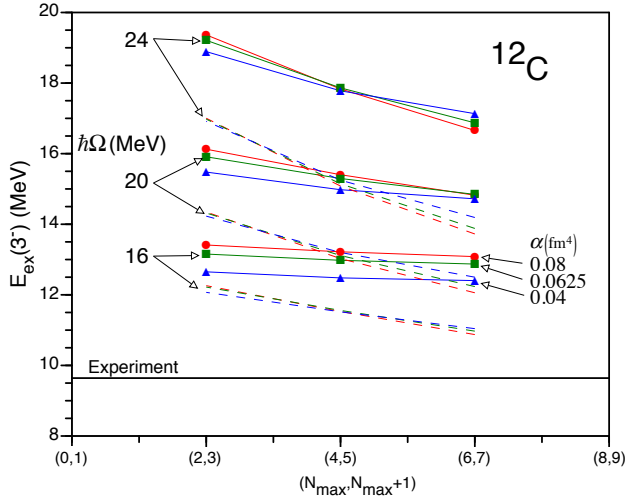


FIG. 6. (color online) Excitation energy of the 3^-0 in ^{12}C as a function of $(N_{\max}, N_{\max} + 1)$ without (dashed lines) and with (solid lines) initial chiral 3N interaction at three different SRG evolution scales and three different HO basis frequencies. The unnatural parity states are computed at $N_{\max} + 1$ while the corresponding excitation energy is calculated with respect to the ground state at N_{\max} so that a pair of basis spaces defines each point in this plot.

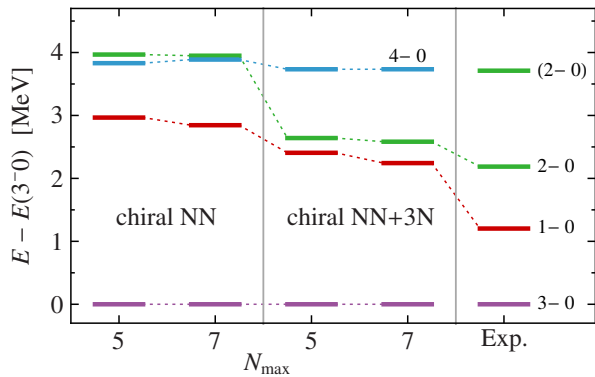


FIG. 7. (color online) Negative parity excitation spectra of ^{12}C obtained without and with initial chiral 3N interaction for two different N_{\max} values, compared with experiment. These NCSM results are calculated at $\hbar\Omega = 20$ MeV for flow parameter $\alpha = 0.0625$ fm⁴.

Finally, we present in Figs. 6 and 7 results for the lowest excited states with negative parity in ^{12}C . Figure 6 displays an array of results for the 3^-0 state from our current investigation, covering the three frequencies $\hbar\Omega = 16, 20,$ and 24 MeV and the three SRG flow parameters $\alpha = 0.04, 0.0625,$ and 0.08 fm⁴. Here we show the energy difference of the 3^-0 state and the 0^+0 ground state obtained in $N_{\max} + 1$ and N_{\max} spaces, respectively.

There is a sizable spread of the excitation energy of the 3^-0 state in Fig. 6 with both frequency and N_{\max} , indicating a slow convergence compared to the typical positive-parity states, both with and without the initial 3N interaction. Nevertheless, our results indicate that the initial chiral 3N interaction increases the excitation energy of the 3^-0 state by a few MeV.

The excitation spectra of the lowest negative parity states relative to the 3^-0 state are better converged, see Fig. 7. Without the chiral 3N interaction the lowest 1^-0 state and even more significantly the 2^-0 states are too high in the negative-parity spectrum. The chiral 3N interaction reduces the excitation energy of both the 1^-0 and 2^-0 states, and brings them in better agreement with the experimental data. Our calculations also indicate that the fourth negative parity state is a 4^-0 state, in agreement with the J^π assignment suggested by Millener [52].

IV. BENCHMARK OF IT-NCSM WITH NCSM

Apart from the discussion of the spectroscopy and other observables of ^{12}C obtained with chiral NN+3N interactions, a second main goal of the present work is to present a benchmark comparison between NCSM and IT-NCSM for ground- and excited-state energies and electromagnetic observables. To this end, Table I contains the numerical results from NCSM and IT-NCSM calculations for our selected ^{12}C observables in a pair-wise comparison.

The general setup of the IT-NCSM calculations presented here is as follows. For basis spaces up to $N_{\max} = (4, 5)$ we use the IT-NCSM code [7, 21] for full NCSM calculations. The energies for these full-space runs agree to within 1 keV and the electromagnetic observables to within 0.1% with the NCSM results obtained with the MFDn code. This establishes a baseline for the numerical precision of the two independent codes, which use the same JT -coupled NN and 3N matrix elements as input.

Beginning at $N_{\max} = 6$, the IT-NCSM calculations involve the importance truncation and threshold extrapolation. A detailed discussion of the IT-NCSM can be found in Refs. [7, 21]. For the positive-parity spectrum, e.g., we target the 8 lowest eigenstates. For each of them we define a reference state by using the corresponding eigenstate obtained in the next-smaller model space and imposing a reference threshold $C_{\min} = 2 \times 10^{-4}$ that eliminated all components with amplitudes below this threshold. This value is expected to be sufficiently small

not to affect the final results, for a detailed analysis see Ref. [21]. These reference states enter into the importance measure used to identify the relevant basis states for the description of any one of the 8 target states, i.e., if the importance measure with respect to at least one reference state is above the importance threshold κ_{\min} the basis state is kept. We employ a sequence of importance thresholds $\kappa_{\min} = \{3, 3.5, 4, \dots, 10\} \times 10^{-5}$ and solve for the eigenvalues within each of the importance-truncated model spaces separately. Based on the energies and observables obtained for the different importance-truncated spaces we perform an extrapolation $\kappa_{\min} \rightarrow 0$. We use a third-order polynomial fit to the results for the full range of importance thresholds with equal weights. The uncertainty of the threshold extrapolation is quantified by changing the order of the polynomial by ± 1 and by excluding the results of the lowest and the lowest two threshold values. The uncertainties quoted in Table I are the standard deviations obtained for this set of extrapolations.

The results of the full NCSM in these larger basis spaces serve as important benchmarks for the IT-NCSM. In general we observe a very good agreement of the IT-NCSM results with the full NCSM with deviations below 1% for almost all cases. Beyond assessing this general agreement, the full NCSM results provide a unique opportunity to test the reliability of the uncertainty estimates obtained from the threshold extrapolation protocol discussed above. It should be noted that we do not account for the numerical uncertainty in the NCSM result used as the benchmark. For energies this NCSM uncertainty is expected to be about 1 keV; for electromagnetic observables the NCSM uncertainty has not been quantified previously, but based on the excellent agreement of the full-space results for $N_{\max} = (4, 5)$ with an independent code we expect uncertainties of the order of the last quoted digit.

Considering all NCSM and IT-NCSM pairs of results in Table I, we observe that the IT-NCSM agrees within the quoted uncertainty with the NCSM result in 60% of the cases. From this observation one might conclude that the procedure used to quantify the IT-NCSM uncertainties is reasonable and may be interpreted in a similar way as a statistical standard deviation. However, there are specific patterns in the size of the estimated uncertainties and the agreement with the full NCSM results.

For the excitation energies of the positive-parity states the estimated IT-NCSM uncertainties resulting from the threshold extrapolation are below 50 keV and the majority of the IT-NCSM results agree with the full NCSM within the estimated uncertainty, though the fraction of cases showing an agreement within the uncertainties decreases significantly for $N_{\max} = 8$ compared to $N_{\max} = 6$.

This is illustrated in Fig. 8, where we display the excitation energies of the positive-parity states obtained in the full NCSM and with the IT-NCSM; the estimated uncertainties of the IT-NCSM are indicated by the boxes. The dashed bars representing the IT-NCSM results al-

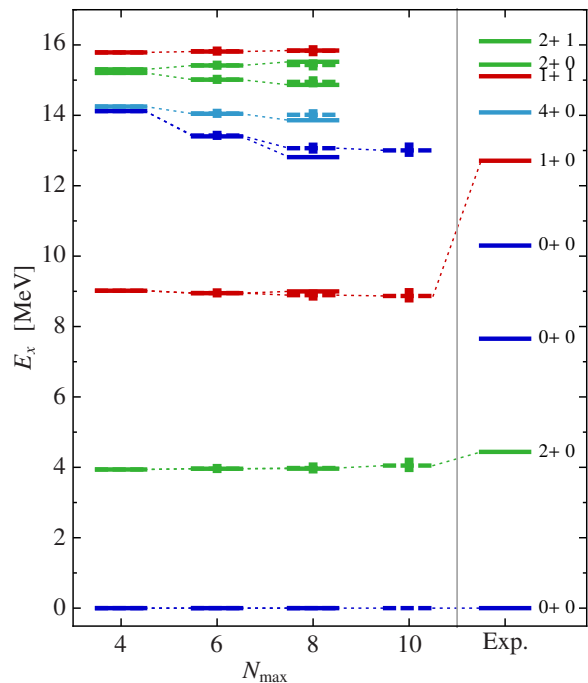


FIG. 8. (color online) Excitation spectra of ^{12}C with the chiral NN+3N interactions, obtained with the NCSM and the IT-NCSM, as a function of N_{\max} , and compared with experiment. The solid lines represent the NCSM result and dashed lines represent the IT-NCSM results, with boxes indicating the typical threshold-extrapolation uncertainties. These results are calculated at $\hbar\Omega = 20$ MeV with the SRG evolution scale $\alpha = 0.0625 \text{ fm}^4$. For $N_{\max} = 10$, only IT-NCSM calculations targeting the lowest four eigenstates are currently available.

most always agree within uncertainties with the solid bars representing the full NCSM. The only case where the difference is more pronounced is the excited 0^+0 . The atypical N_{\max} dependence of this state already hints at a complicated structure of the wave function which is dominated by small components—evidently this represents a more difficult situation for the importance truncation and threshold extrapolation. For completeness we also show excitation energies at $N_{\max} = 10$, which were obtained in an IT-NCSM calculation targeting the four lowest eigenstates.

For the excitation energies of the negative-parity states relative to the 3^-0 state, as shown in Fig. 9, the agreement of the IT-NCSM and the full NCSM is equally good. Based on the direct threshold extrapolation of the excitation energies within the negative-parity space, the uncertainties of the IT-NCSM energies are comparable to the uncertainties of the positive-parity excitation energies. Note, however, that the uncertainties of excitation energies of the negative-parity states relative to the positive-parity ground state, as reported in Table I, are significantly larger. This results from the larger uncertainties of the threshold extrapolations for the absolute energies of the 3^-0 and the 0^+0 states needed to deter-

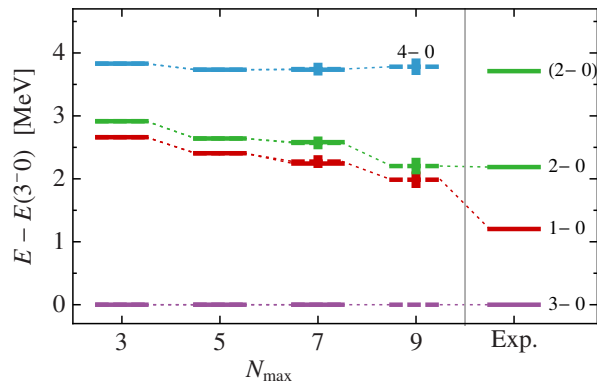


FIG. 9. (color online) Excitation of the negative parity spectra of ^{12}C with respect to the lowest 3^-0 state using the chiral NN+3N interaction, obtained with the NCSM and the IT-NCSM, as a function of N_{\max} , and compared with experiment. The solid lines represent the NCSM result and dashed lines represent the IT-NCSM results. These results are calculated at $\hbar\Omega = 20$ MeV with the SRG evolution scale $\alpha = 0.0625 \text{ fm}^4$. For $N_{\max} = 9$, only IT-NCSM calculated eigenstates are currently available.

mine the offset of the negative-parity with respect to the positive-parity spectrum. The uncertainties in this offset induce sizeable systematic uncertainties in the excitation energies of the negative-parity states, as seen in Table I.

For radii and electromagnetic observables the threshold extrapolations typically produce larger error bars, particularly for long-range observables like the radii or quadrupole moments and transitions. Nevertheless, even for these observables, the results in Table I show that the NCSM and IT-NCSM results fall within the quoted IT-NCSM uncertainty in the majority of cases.

There is a systematic trend in uncertainties of the IT-NCSM results when going from $N_{\max} = (6, 7)$ to $N_{\max} = (8, 9)$. First of all, the uncertainty estimates increase with increasing N_{\max} . This is due to the fact that the IT-NCSM space covers a smaller fraction of the complete N_{\max} space so that the threshold extrapolation has to account for the contribution of a larger fraction of discarded basis states. Second, the fraction of cases in which the IT-NCSM agrees with the NCSM within the uncertainties is reduced for $N_{\max} = (8, 9)$. This might be explained by uncertainties that are not accounted for by the threshold extrapolation and uncertainty quantification protocol. An example are inaccuracies resulting from building the importance-truncated space for $N_{\max} = (8, 9)$ on reference states that already result from an importance-truncated $N_{\max} = (6, 7)$ calculation—the uncertainties inherited from the $N_{\max} = (6, 7)$ states and the additional reference threshold C_{\min} are not yet accounted for by the $N_{\max} = (8, 9)$ uncertainty estimate. Since a numerical propagation of these uncertainties is computationally expensive, one might consider other threshold extrapolation schemes that are robust in this respect. A promising candidate is a threshold extrapolation based on the energy variance [53, 54] and studies along these

lines are in progress.

These benchmark comparisons show that the intrinsic uncertainty estimates extracted from the threshold extrapolation provide a suitable guideline for the accuracy of the IT-NCSM results. However, one has to keep in mind that the estimates do not capture the accumulation of uncertainties throughout a sequence of importance truncated calculations with increasing N_{\max} . The relative size of the uncertainties depends on the observable and the structure of the states. If the resulting uncertainty appears too large for a specific application, one may elect to decrease the importance thresholds, which is guaranteed to improve the results and reduce the extrapolation uncertainties.

V. SUMMARY AND CONCLUSIONS

We have presented *ab initio* NCSM and IT-NCSM calculations of ^{12}C using SRG-evolved chiral NN+3N Hamiltonians. Both, spectra and electromagnetic properties are examined as a function of the SRG flow-parameter as well as a function of the model-space parameters ($N_{\max}, \hbar\Omega$). We have extended previous investigations with the same Hamiltonian to larger model spaces and to a larger set of observables. Furthermore, we have benchmarked the IT-NCSM with the NCSM in model spaces where the latter is feasible.

For most low-lying positive-parity states the excitation energies are reasonably well converged, though noticeable exceptions are the first excited 0^+0 state (the Hoyle state) and the first 0^+1 state. Indeed, it is known that in order to converge the Hoyle state one needs significantly larger model spaces. Electromagnetic observables such as magnetic moments and M1 transition strengths are also reasonably well converged, but quadrupole moments and E2 transitions are not yet converged, even in the largest model spaces that we have considered here. This should however not be surprising, since the E2 operator is a long-range operator, and hence convergence is notoriously slow in a HO basis.

The comparison of our theoretical spectra with experiment reveals some remarkable points. For most of the positive-parity states the excitation energies obtained without the initial chiral 3N interaction are in good qualitative agreement with experiment. Typically the agreement is improved by including the chiral 3N interaction, in particular for the rotational excitations, the lowest 2^+0 and 4^+0 states. Also the 0^+1 state is very sensitive to the 3N interaction, and in better agreement with experiment than without the 3N interaction. A surprising exception is the 1^+0 state. It is in good agreement with experiment without the chiral 3N interaction. However, with the chiral 3N interaction the excitation energy is pushed about 4 MeV below the experimental value.

The excitation energies of the lowest excited negative-parity states with respect to the 3^-0 state (the lowest negative-parity state) are also reasonably well converged.

However, the negative-parity states converge slower than the positive-parity states in terms of absolute energies, and hence the excitation energies of the negative-parity states are not converged with respect to the ground state. Nevertheless, it appears that the dominant effect of the chiral 3N interaction on the negative-parity states is an overall upward shift of the states with respect to the positive-parity ground state.

The excitation energies of the 1^{+0} state and the 0^{+1} state represent valuable test cases for next-generation (chiral) Hamiltonians. The failure of the present chiral NN at N^3LO plus 3N interaction at N^2LO to quantitatively capture the physics of these states represents a challenge for improved chiral interactions, in particular the 3N interaction at N^3LO [55, 56]. Further detailed investigations into the structure of these states and their sensitivity to different existing chiral NN+3N interactions are in progress.

In terms of enlarging the model space, which may be necessary in order to address these issues, there are alternatives to the straightforward but challenging task of enlarging the HO basis itself. In particular, it may be more fruitful to adopt another basis with improved infrared properties such as the Coulomb-Sturmian basis [57–59]. Alternatively, it may be more efficient to remain within the HO basis (thereby preserving factorization of the center-of-mass motion) but selecting symmetry-adapted basis spaces such as those recently advocated for light nuclei [41] and especially for ^{12}C [60, 61]. Another avenue is the explicit treatment of clusters and their relative motion in the NCSM with continuum (NCSMC) that was recently formulated and successfully applied to the de-

scription of the unbound nucleus 7He [62].

ACKNOWLEDGMENTS

This work was supported in part by the US National Science Foundation under Grant No. PHY-0904782, the US Department of Energy (DOE) under Grant No. DE-FG02-87ER40371 and DESC0008485 (SciDAC-3/NUCLEI), by the Deutsche Forschungsgemeinschaft through contract SFB 634, by the Helmholtz International Center for FAIR (HIC for FAIR) within the LOEWE program of the State of Hesse, and the BMBF through contract 06DA7047I. This work was supported partially through GAUSTEQ (Germany and U.S. Nuclear Theory Exchange Program for QCD Studies of Hadrons and Nuclei) under contract number DESC0006758. A portion of the computational resources were provided by the National Energy Research Scientific Computing Center (NERSC), which is supported by the US DOE Office of Science, and by an INCITE award, "Nuclear Structure and Nuclear Reactions", from the US DOE Office of Advanced Scientific Computing. This research also used resources of the Oak Ridge Leadership Computing Facility at ORNL, which is supported by the US DOE Office of Science under Contract DE-AC05-00OR22725. Further resources were provided by the computing center of the TU Darmstadt (lichtenberg), the Jülich Supercomputing Centre (juropa), and the LOEWE-CSC Frankfurt.

-
- [1] P. Navratil, J. Vary, and B. Barrett, Phys. Rev. Lett. **84**, 5728 (2000).
 - [2] P. Navratil, J. P. Vary, and B. R. Barrett, Phys. Rev. C **62**, 054311 (2000).
 - [3] B. R. Barrett, P. Navratil, and J. P. Vary, Prog. Part. Nucl. Phys. **69**, 131 (2013).
 - [4] P. Maris, J. P. Vary, and A. M. Shirokov, Phys. Rev. C **79**, 014308 (2009).
 - [5] P. Navratil, S. Quaglioni, I. Stetcu, and B. R. Barrett, J. Phys. G **36**, 083101 (2009).
 - [6] P. Maris, A. Shirokov, and J. Vary, Phys. Rev. C **81**, 021301 (2010).
 - [7] R. Roth, Phys. Rev. C **79**, 064324 (2009).
 - [8] R. Roth, J. Langhammer, A. Calci, S. Binder, and P. Navratil, Phys. Rev. Lett. **107**, 072501 (2011).
 - [9] R. Roth, S. Binder, K. Vobig, A. Calci, J. Langhammer, and P. Navratil, Phys. Rev. Lett. **109**, 052501 (2012).
 - [10] P. Maris, J. Vary, P. Navratil, W. Ormand, H. Nam, and D. Dean, Phys. Rev. Lett. **106**, 202502 (2011).
 - [11] P. Navratil and S. Quaglioni, Phys. Rev. Lett. **108**, 042503 (2012).
 - [12] E. Epelbaum, H.-W. Hammer, and U.-G. Meißner, Rev. Mod. Phys. **81**, 1773 (2009).
 - [13] R. Machleidt and D. R. Entem, Phys. Rep. **503**, 1 (2011).
 - [14] S. D. Glazek and K. G. Wilson, Phys. Rev. D **48**, 5863 (1993).
 - [15] F. Wegner, Ann. Phys. **506**, 77 (1994).
 - [16] S. K. Bogner, R. J. Furnstahl, P. Maris, R. J. Perry, A. Schwenk, and J. P. Vary, Nucl. Phys. A **801**, 21 (2008).
 - [17] S. K. Bogner, R. J. Furnstahl, and A. Schwenk, Prog. Part. Nucl. Phys. **65**, 94 (2010).
 - [18] R. Furnstahl, Nucl. Phys. Proc. Suppl. **228**, 139 (2012).
 - [19] E. D. Jurgenson, P. Navratil, and R. J. Furnstahl, Phys. Rev. Lett. **103**, 082501 (2009).
 - [20] E. Jurgenson, P. Maris, R. Furnstahl, P. Navratil, W. Ormand, *et al.*, Phys. Rev. C **87**, 054312 (2013).
 - [21] R. Roth, A. Calci, J. Langhammer, and S. Binder, (2013), arXiv:1311.3563 [nucl-th].
 - [22] P. Maris, H. M. Aktulga, S. Binder, A. Calci, U. V. Catalyürek, J. Langhammer, E. Ng, E. Saule, R. Roth, J. P. Vary, and C. Yang, J. Phys. Conf. Ser. **454**, 012063 (2013).
 - [23] D. R. Entem and R. Machleidt, Phys. Rev. C **68**, 041001 (2003).
 - [24] E. Epelbaum, A. Nogga, W. Gloeckle, H. Kamada, U.-G. Meißner, and H. Witala, Phys. Rev. C **66**, 064001 (2002).

- [25] P. Navratil, *Few Body Syst.* **41**, 117 (2007).
- [26] D. Gazit, S. Quaglioni, and P. Navratil, *Phys. Rev. Lett.* **103**, 102502 (2009).
- [27] E. Jurgenson, P. Navratil, and R. Furnstahl, *Phys. Rev. C* **83**, 034301 (2011).
- [28] D. Gazit, S. Quaglioni, and P. Navratil, *Phys. Rev. Lett.* **103**, 102502 (2009).
- [29] P. Navratil, V. G. Gueorguiev, J. P. Vary, W. E. Ormand, and A. Nogga, *Phys. Rev. Lett.* **99**, 042501 (2007).
- [30] S. Okubo, *Prog. Theor. Phys.* **12**, 603 (1954).
- [31] K. Suzuki and S. Y. Lee, *Prog. Theor. Phys.* **64**, 2091 (1980).
- [32] R. Roth, T. Neff, and H. Feldmeier, *Prog. Part. Nucl. Phys.* **65**, 50 (2010).
- [33] P. Navratil, G. P. Kamuntavicius, and B. R. Barrett, *Phys. Rev. C* **61**, 044001 (2000).
- [34] D. Orsypayev, H. Potter, P. Maris, M. Sosenkina, J. P. Vary, S. Binder, A. Calci, J. Langhammer, and R. Roth, *IEEE 27th Parallel and Distributed Processing Symposium Workshops & PhD Forum (IPDPSW)*, 1365 (2013).
- [35] H. Potter, D. Orsypayev, P. Maris, M. Sosenkina, J. P. Vary, S. Binder, A. Calci, J. Langhammer, R. Roth, U. Catalyurek, and E. Saule, *Proceedings of International Conference 'Nuclear Theory in the Supercomputing Era - 2013' (NTSE-2013)*, Ames, IA, USA, May 13-17, 2013. Eds. A. M. Shirokov and A. I. Mazur. Pacific National University, Khabarovsk, Russia, 263 (2014).
- [36] P. Sternberg, E. G. Ng, C. Yang, P. Maris, J. P. Vary, M. Sosenkina, and H. V. Le, in *SC (IEEE/ACM, 2008)* p. 15.
- [37] P. Maris, M. Sosenkina, J. P. Vary, E. G. Ng, and C. Yang, *Procedia CS* **1**, 97 (2010).
- [38] H. M. Aktulga, C. Yang, E. G. Ng, P. Maris, and J. P. Vary, in *Euro-Par*, *Lecture Notes in Computer Science*, Vol. 7484, edited by C. Kaklamanis, T. S. Papatheodorou, and P. G. Spirakis (Springer, 2012) pp. 830–842.
- [39] P. Maris, H. Aktulga, M. Caprio, U. Catalyurek, E. Ng, D. Orsypayev, H. Potter, E. Saule, M. Sosenkina, J. Vary, C. Yang, and Z. Zhou, *J. Phys. Conf. Ser.* **403**, 012019 (2012).
- [40] M. Caprio, P. Maris, and J. Vary, *Phys. Lett. B* **719**, 179 (2013).
- [41] T. Dytrych, K. D. Launey, J. P. Draayer, P. Maris, J. P. Vary, E. Saule, U. Catalyurek, M. Sosenkina, D. Langr, and M. A. Caprio, *Phys. Rev. Lett.* **111**, 252501 (2013).
- [42] M. Chernykh, H. Feldmeier, T. Neff, P. von Neumann-Cosel, and A. Richter, *Phys. Rev. Lett.* **98**, 032501 (2007).
- [43] T. Neff, *J. Phys. Conf. Ser.* **403**, 012028 (2012).
- [44] E. Epelbaum, H. Krebs, D. Lee, and Ulf-G. Meißner, *Phys. Rev. Lett.* **106**, 192501 (2011).
- [45] E. Epelbaum, H. Krebs, T. A. Lahde, D. Lee, and Ulf-G. Meißner, *Phys. Rev. Lett.* **109**, 252501 (2012).
- [46] Developments along these lines are ongoing within the LENPIC collaboration. See <http://www.lenpic.org>.
- [47] F. Ajzenberg-Selove, *Nuclear Physics A* **506**, 1 (1990).
- [48] H. D. Vries, C. D. Jager, and C. D. Vries, *Atomic Data and Nuclear Data Tables* **36**, 495 (1987).
- [49] W. Vermeer, M. Esat, J. Kuehner, R. Spear, A. Baxter, and S. Hinds, *Phys. Lett. B* **122**, 23 (1983).
- [50] A. Hayes, P. Navratil, and J. Vary, *Phys. Rev. Lett.* **91**, 012502 (2003).
- [51] S. Coon and H. Han, *Few Body Syst.* **30**, 131 (2001).
- [52] D. Millener, comment in NNDC data base regarding suggested 4^- assignment for state in ^{12}C spectra.
- [53] H. Zhan, A. Nogga, B. R. Barrett, J. P. Vary, and P. Navrátil, *Phys. Rev. C* **69**, 034302 (2004).
- [54] T. Abe, P. Maris, T. Otsuka, N. Shimizu, Y. Utsuno, *et al.*, *Phys. Rev.* **C86**, 054301 (2012).
- [55] V. Bernard, E. Epelbaum, H. Krebs, and U.-G. Meißner, *Phys. Rev. C* **77**, 064004 (2008).
- [56] V. Bernard, E. Epelbaum, H. Krebs, and U.-G. Meißner, *Phys. Rev.* **C84**, 054001 (2011).
- [57] B. Keister and W. Polyzou, *J. Comput. Phys.* **134**, 231 (1997).
- [58] M. Caprio, P. Maris, and J. Vary, *Phys. Rev. C* **86**, 034312 (2012).
- [59] M. Caprio, P. Maris, and J. Vary, *J. Phys. Conf. Ser.* **403**, 012014 (2012).
- [60] A. C. Dreyfuss, K. D. Launey, T. Dytrych, J. P. Draayer, and C. Bahri, *Phys. Lett.* **B727**, 511 (2013).
- [61] T. Dytrych, P. Maris, K. D. Launey, J. P. Draayer, J. P. Vary, M. A. Caprio, D. Langr, U. V. Catalyurek, E. Saule, and M. Sosenkina, (2014), in preparation.
- [62] S. Baroni, P. Navrátil, and S. Quaglioni, *Phys. Rev. Lett.* **110**, 022505 (2013).